Chapter 2
A Quick Look on Small Scale Flux Tubes

Abstract In this chapter we recall some basic steps of how magnetic flux tubes were discovered and how they were viewed in their early years. During the decades after their discovery, flux tubes evolved from an interesting novelty into a founding element of solar magnetism. Today, we know that the entire magnetic field of the Sun, from sunspots to coronal loops and solar wind, has a filamentary structure. We briefly discuss the universality of filamentary structures in universe.

2.1 Early Years

For ages, solar magnetic fields were associated with sunspots. The existence of magnetic field concentrations outside sunspots has been realized only in the late 1950s. Howard (1959), observing magnetic fields in various active and quiet sun regions, found that existence of magnetic "features" with fields greater than 75 G outside sunspots and far removed from them, is "not uncommon." Confirming the correspondence between calcium bright points (seen at chromospheric temperatures) and photospheric magnetic fields, described earlier by Babcock and Babcock (1955), Howard writes: "A close correspondence in most small structural details between the calcium plages and magnetic field tends to indicate a real physical relationship between the two," and finally suggests that "the magnetic field in the solar photosphere and chromosphere is in the form of more or less *vertical columns*."

Leighton (1959) describing his observations of magnetic field in plage regions also concludes that "relatively strong field, 100 or 200 G in strength are found in extensive areas throughout plage regions, the field pattern being in striking agreement with the pattern of Ca II emission."

The same year, Severny (1959) reports on the observations of fine structures in *sunspots*!

Such was the birth of small scale magnetic flux tubes. Not only were the existence of small scale magnetic features detected, but they were found uniquely associated with two important phenomena. One was a direct correlation with heating the overlying chromosphere (Ca II emission), and the other was formation of large-scale magnetic shear formed all over the solar surface by small scale "columns" of opposite polarity.

M. Ryutova, *Physics of Magnetic Flux Tubes*, Astrophysics and Space Science Library 417, DOI 10.1007/978-3-662-45243-1_2

Pikel'ner (1963), well before the small scale flux tubes were directly observed, was the first to predict the existence of flux tubes. He suggested that convective motions acting on the magnetic lines of force, squeeze them and crowd in toward the periphery of the granules, and that the field becomes concentrated into a network covering the sun's surface. He also predicted that the enhanced convection contributes to chromospheric emission, so that the network becomes observable in Ca II and Hα lines. Moreover, Pikel'ner found that the motion of plasma entrained in the magnetic field lines is responsible for the observed mottles consisting of granular elements streaming from the center toward the periphery, and concluded that the presence of mottling over the entire solar surface demonstrates that a "weak" field exists everywhere. The direct observation of these suggestions were still to come.

2.1.1 First Direct Observational Signs of Magnetic Flux Tubes

Using the photographic technique of Leighton for high spatial resolution measurements of photospheric magnetic fields, Sheeley (1966, 1967) finds that as a bipolar magnetic region develops in time and as its magnetic flux spreads over a larger area, the flux density does not decrease smoothly, but is distributed in bits and fragments of progressively smaller sizes until finally, they escape detection below the threshold of photographic measurements. The magnetic field in these small magnetic features was found to range from 200 to 700 G. Sheeley states that "wherever there are adjacent regions of opposite polarity, there are disk filaments in Hα." His conclusion, that "magnetic fields of several hundred gauss occur in tiny areas easily as small as 500 km in regions of the solar surface sometimes well removed from sunspot activity," became the turning point which, despite the predecessors, is a fact of the discovery of small scale flux tubes.

Just at about the same time, observing magnetic fields of small sunspots and pores, Steshenko (1967) finds that the field strength of the smallest pores ($1'' - 0.5{-}2''$) is about 1,400 G. In larger spots he finds very small elements with a field strength of 5,350 G (!), much higher than the average field of the sunspot itself. He also observed an isolated places outside sunspots having field strengths up to 1,000 G.

Beckers and Schröter (1968) performed an extremely detailed study of the small scale magnetic structures *in* and *around* the sunspots. These studies included the measurements of velocity, intensity, and magnetic field strength in the fine elements. By these observations they confirmed and extended Sheeley' findings, providing substantial guideline for future observations. Being quite cautious, they start the discussion as follows: "We presented in this paper evidence that most, and perhaps all, of the photospheric magnetic field around an unipolar sunspot is concentrated in a few thousand small region (1,000 km in diameter) with strong magnetic fields (up to 1,400 G). This, together with the other properties of the magnetic knots, shows that they are an essential part of a solar activity regions. We are, however, not yet able to decide definitely whether they occur only in the dissolution phase or whether they are a permanent constituent of a solar activity region."

Soon, it was found that almost the entire surface outside sunspots is covered by small scale magnetic elements. Howard and Stenflo (1972), analyzing Mount Wilson magnetogram recordings obtained during 26 days with 17 by 17 arcsec aperture, found that more than 90 % of the total flux is channeled through narrow flux tubes with very high field strength in plages and at the boundaries of supergranular cells. The flux tubes occupying a very small region in the photosphere were found rapidly spreading out with height. This spreading of the field lines and decreasing the field strength with height was dabbed the "mushroom effect," described earlier by Pikel'ner (1963) as chromospheric mottling (Frazier and Stenflo 1972).

2.1.2 The Sunspot Dilemma

It is interesting that just before these fundamental results establishing the filamentary structure of sun's magnetic fields outside sunspots, and long before the recent high-resolution observations, Papathanasoglou (1971), along the earlier findings of Crimea group (see e.g. Severny 1959), has observed the filamentary structure of *sunspot umbra*, and showed that the widths of umbral filaments are $<1''$, and that dark spacing between them are about 0.6." This amazing result was totally ignored, earning only three (!) citations, first of which was given by Livingston (1991) in his Nature article "Radial Filamentary Structure in a Sunspot Umbra," where he also reports on the direct observations of the filamentary structure of sunspot umbra.

For many years, however, the study of small scale filamentary structure of umbrae was overshadowed by studies of a sunspot as a whole, its stability and its impact on the surrounding and overlying atmosphere. The large-scale observational data clearly indicated that as a whole, the sunspots must be intrinsically unstable. The stability analysis of such a complex and ever changing body requires consideration of many competing effects—the job that yet has to be done. And search for the mechanisms of sunspot stability became an uphill battle. The filamentary structure of the sunspot body has been put aside by the majority of researchers. The most revealing of the acute situation of those days is, probably, an example of Piddington's research.

The large body of Piddington's work on solar magnetic fields may be characterized by his own words (1975): "A phenomenological model of solar magnetic fields is developed, which differs drastically from all currently popular (diffuse-field) models. Its acceptance would require a review of a major part of theoretical solar physics."

Revision of a major part of solar theories and interpretations was not easy, and Piddington's ideas in many aspects of solar magnetism caused various reactions, from such definitions as "Piddington's Heresy" (Parker (1976) on role of turbulent diffusion) to a silent dropping off his works from citations. Figure 2.1 shows an example of the Piddington's model of sunspot consisting of the individual twisted flux tubes.

Meyer et al. (1977) reacted to Piddington's model of sunspot stability simply: "We shall show, using a simplified model, that a sunspot can be stable in and immediately below the photosphere. This stability can be related to the potential energy associated with the Wilson depression. *There is no need to invoke twisted fields* (e.g. Piddington (1975)), *which have not been observed.*" (!)

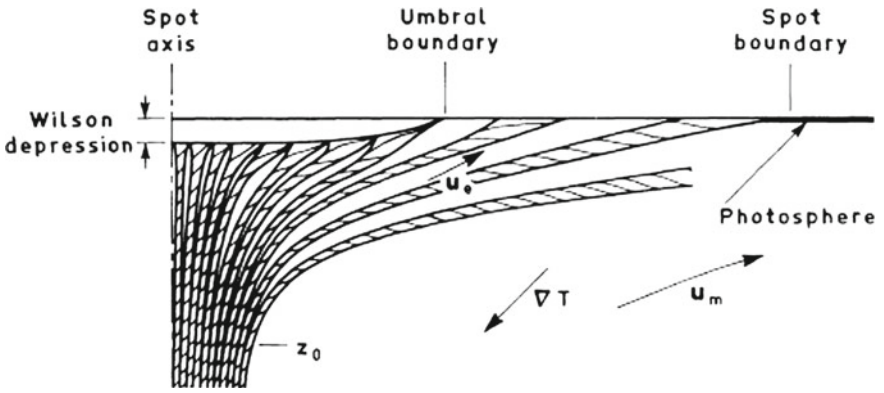

Fig. 2.1 Section of a sunspot magnetic field with the flux-rope helical twist omitted for simplicity. The individual flux tubes are shown twisted and separated by nonmagnetic plasma regions whose width increases with distance from the axis, thus accounting for the penumbral filaments. the Evershed flow u_e has different directions and velocities inside and outside the flux tubes. Reprinted from Piddington (1978) by permission from Springer Science and Business Media

By the time of this statement, from a basic plasma theory, supported by laboratory experiments, it was already well known that long magnetic cylinders are intrinsically unstable with respect to so-called screw-pinch instability (Shafranov 1956; Kruskal and Kulsrud 1958; Kadomtsev 1966). A condition for screw-pinch instability, known as Kruskal-Shafranov condition, is simple: flux tube with magnetic field $\mathbf{B}(0, B_\phi, B_z)$, radius R and length L, will be inevitably twisted if

$$q = \frac{2\pi R B_z}{L B_\phi} \equiv \frac{h}{L} < 1, \tag{2.1}$$

where q is the safety factor, and h is the pitch of helical configuration, i.e., the distance in which the field line makes one revolution around the flux tube. In case of solar magnetic flux tubes, the safety factor is always <1, which means that any magnetic flux confined in a cylinder with roughly $R \ll L$ must be twisted. Indeed, high-resolution observation shows that magnetic flux tubes, sunspots, ropes and loops are intrinsically twisted. And Kruskal-Shafranov condition is fulfilled for prevailing majority of solar magnetic structures. We will see throughout the book how well this feature is observed, and what an important role is played by screw-pinch instability in properties and dynamics of various regions of solar atmosphere.

One can say that at those times Piddington's model of solar magnetic fields including sunspots (Fig. 2.1), active regions and their environments, based on the model of twisted flux ropes, was too ahead of time and probably the closest to the goal. More general features of solar magnetic field visualized by Piddington (1978) are shown in Fig. 2.2. All these features, as already mentioned, have been subsequently confirmed (Ryutova et al. 2008; Su et al. 2010; Ruiz Cobo and Puschmann 2012; Stenflo 2013).

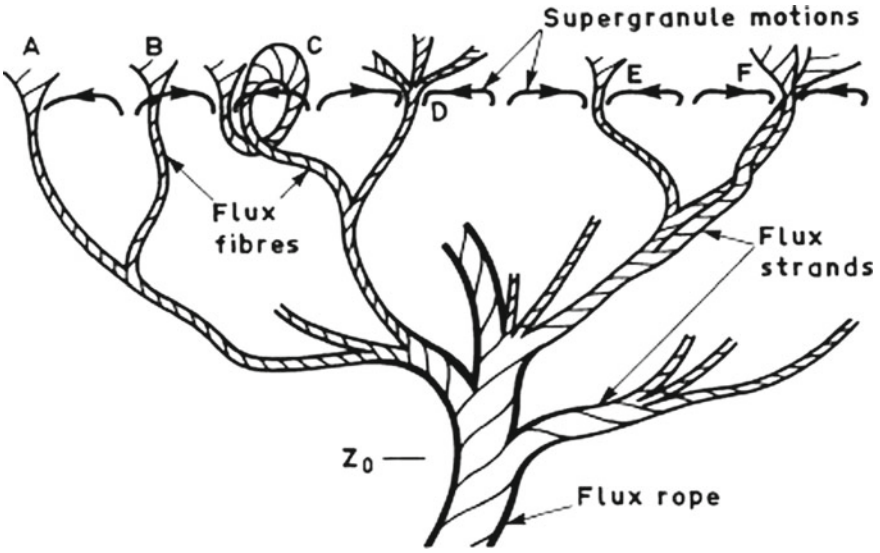

Fig. 2.2 Schematic of the main magnetic and plasma features of decaying active regions and quiet sun. The flux-rope section acts as the trunk of a tree-like structure whose main branches are flux strands. These, in turn, fray into flux fibers ($\simeq 3 \times 10^{18}$ Mx) which provide the network rosettes (on disk) and bushes (at limb). These tend to be driven to the supergranular boundaries (*A*), but may be observed piercing the cell interior (*B*). The kink instability provides a loop (*C*). A flux fiber frays further (*D*) into flux threads ($\simeq 3 \times 10^{17}$ Mx) which provide the photospheric filigree and chromospheric mottles. A group of flux fibers (*E*) and perhaps some flux strands (*F*) form a boundary and force a convective cell to turn over continuously for several days. Reprinted from Piddington (1978) by permission from Springer Science and Business Media

2.2 Elements of Theory for de Facto Flux Tubes

The theoretical approach to the origin and properties of small scale magnetic flux tubes started to flourish only in the middle of 70s. By that time, a decade of efforts of observers prepared a rich ground for these studies.

Parker (1974a, b) proposed a simple hydrodynamic mechanism associated with turbulent pumping to squise magnetic field into the slender tube (Fig. 2.3). He writes: "The obvious point of departure for an inquiry into the origin of intense fields in the supergranular boundaries is the well-known effect in which the outflow of fluid from the center of each supergranular sweeps the vertical component of magnetic field to the boundary." The key element in this scheme is that the turbulent pumping of fluid downward at the supergranular boundary produces a partial vacuum within the flux tubes, just like in the water jet vacuum pump, in which one fluid is forced along by turbulent coupling to another. In this scheme, the field is restricted by energy equipartition, $B^2/8\pi \simeq (1/2)\rho v^2$, and limits the value of the magnetic field by a maximum of about 500 G. Uncertainty in velocity fields and too low value of the magnetic field leads Parker to add yet another effect that is supposed to further concentrate the

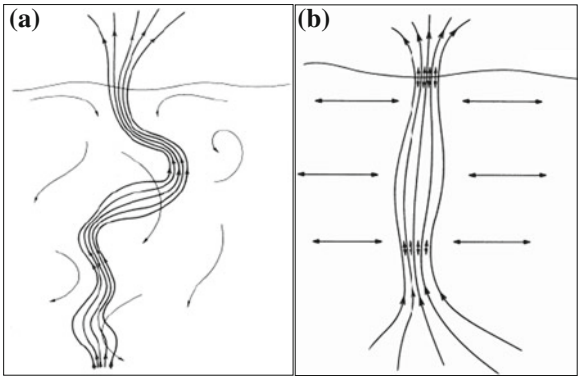

Fig. 2.3 Sketch of a magnetic flux tube extending up through the photosphere. **a** Turbulent subsiding fluid in a supergranular boundary into the tenuous chromosphere above the visible surface of the sun. **b** The magnetic field lines alternately squeezed and expanded in the turbulent convection beneath the photosphere, causing the surge up and down along the flux tube; the open ends are indicated by the *short double arrows*. Reprinted from Parker (1974a, b) by permission from IOP, AAS

individual flux tubes, namely the Bernoulli effect. Unfortunately, this effect increases the mean magnetic field only to a fraction of the equipartition value. And Parker concludes that "we must look farther" (Parker (1974b), see also Parker (1979)).

The origin of the small scale magnetic flux tube covering the entire solar surface and making up sunspots, plages, and active regions is still an open question.

It is therefore not surprising that the first theoretical works on fundamental properties of flux tubes were based on their de facto existence (Cram and Wilson 1975; Ryutov and Ryutova 1976; Defouw 1976; Ryutova 1977; Roberts and Webb 1978; Spruit 1981).

The basic equations employed in early attempts to study properties of magnetic flux tubes are Maxwell equations mainly in the MHD approximation:

$$\nabla \cdot \mathbf{B} = 0 \tag{2.2}$$

$$\frac{\partial \mathbf{B}}{\partial t} = \nabla \times (\mathbf{v} \times \mathbf{B}) + \eta_D \nabla^2 \mathbf{B} \tag{2.3}$$

$$\rho \frac{\mathrm{d}\mathbf{v}}{\mathrm{d}t} = -\nabla p + \frac{1}{4\pi}(\nabla \times \mathbf{B}) \times \mathbf{B} - \rho g(z) \tag{2.4}$$

$$\frac{\mathrm{d}\rho}{\mathrm{d}t} + \rho \nabla \cdot \mathbf{v} = 0 \tag{2.5}$$

$$\frac{\partial(\rho^{-\gamma} p)}{\partial t} + \mathbf{v} \nabla (\rho^{-\gamma} p) = 0 \tag{2.6}$$

where $\mathrm{d}/\mathrm{d}t$ designates a full derivative ($\mathrm{d}/\mathrm{d}t = \partial/\partial t + \mathbf{v} \cdot \nabla$), $\eta_D = c^2/4\pi\sigma$ is magnetic diffusivity, and $\sigma = 1.96 ne^2/(m_\mathrm{e}\nu_\mathrm{ei})$ is the plasma conductivity.

The magnetic flux tube, in a simple cylindrically symmetric model, may be considered as a set of magnetic field lines through some surface S bounded by the closed contour C. The lines of force are defined in terms of $\mathbf{B}(\mathbf{r})$, as the solution of equations

$$\frac{\mathrm{d}r}{B_r} = \frac{r\mathrm{d}\phi}{B_\phi} = \frac{\mathrm{d}z}{B_z} \tag{2.7}$$

Applying Gauss's theorem to (2.2) we see that the total magnetic flux across any closed surface S is zero,

$$\int_S \mathbf{B} \cdot \mathbf{dS} = 0, \tag{2.8}$$

which means that every line of force entering S must also leave, i.e., the individual lines either extend to infinity or form closed curves. It follows then that the total number of lines, i.e., the total magnetic flux through any closed contour C is constant and can be written as

$$\Phi = \int_C \mathbf{B} \cdot \mathbf{dS} \tag{2.9}$$

which means, for example, that the strength of a flux tube increases when it narrows and decreases when it widens.

Let us now turn to question what are the requirements for the equilibrium of a flux tube. Consider the simplest case of hydrostatic equilibrium and assume that the magnetic field depends only on coordinate r, $\mathbf{B} = B(0, 0, B_z(r))$. Equation (2.4), that provides the momentum balance, is then

$$-\nabla p + \frac{1}{4\pi}(\nabla \times \mathbf{B}) \times \mathbf{B} - \rho \boldsymbol{g} = 0 \tag{2.10}$$

In an absence of gravity from this equation we have

$$p(r) + \frac{B_z^2(r)}{8\pi} = p_\mathrm{e} \tag{2.11}$$

$$p(r) + \frac{B_z^2(r)}{8\pi} = p_\mathrm{e} + \frac{B_{z\mathrm{e}}^2(r)}{8\pi}$$

where the constant of integration, p_e is obviously a gas pressure outside the flux tube, p_e, in case if flux tube is embedded in magnetic free environment, $p_\mathrm{e} + B_{z\mathrm{e}}^2/8\pi$, if the magnetic field outside flux tube is nonzero. Equations (2.11) are classical conditions for static equilibrium of magnetic flux tube.

In the presence of gravity, if it acts along the negative direction of z-axis, (2.10) gives:

$$\frac{\mathrm{d}p}{\mathrm{d}z} + \rho g(z) = 0 \tag{2.12}$$

Taking into account the ideal gas low, $\rho = mp/kT$ (k is Boltzmann constant) we have

$$p = p_0 \exp\left(-\int_0^z \frac{1}{\Lambda(z)} \mathrm{d}z\right) \tag{2.13}$$

where

$$\Lambda(z) = \frac{kT}{mg} \tag{2.14}$$

is the pressure scale height. In terms of density, (2.13) becomes

$$\rho = \rho_0 \frac{T_0}{T(z)} \exp\left(-\int_0^z \frac{1}{\Lambda(z)} \mathrm{d}z\right) \tag{2.15}$$

It is important to note that MHD equations (2.2)–(2.6) allow to study quite a limited classes of phenomena. Throughout this book, however, we will encounter the problems that will require much more elaborated approach. In each particular case, for example, such as nonlinear unsteady phenomena, dynamics of nonconservative systems, self-organized processes and many others, we will deal with the special technique.

2.3 Numerical Visualization and Observations

One of the first exemplary models of a quasi-static flux tube was constructed numerically by Deinzer et al. (1984a, b). The full MHD equations for a compressible medium together with an energy equation were solved in two-dimensional geometry for a slender slab being in the pressure equilibrium with surrounding plasma. It was assumed that all quantities have a barometric dependence on z; cf. (2.13).

Figure 2.4 shows an example of the numerical solution for density, magnetic field and velocity at a time when stationary state has been evolved (half of the symmetric structure is shown). The important results obtained in this calculation are, for example, that the density is reduced inside the slab to half of the ambient plasma, and appearence of downflows around the magnetic slab caused by noncollinearity of the isotherms and lines of constant gravitational potential (not shown). Even these relatively early modeling (although only two dimensional) quite adequately represent what is to be observed. The results of more advanced numerical simulations of flux tube structures and additional literature can be found, for example, in Steiner (2007).

High-resolution observation with ground-based and space telescopes have allowed to study the inner structure of small scale flux tubes and their chromospheric counterparts seen as bright points.

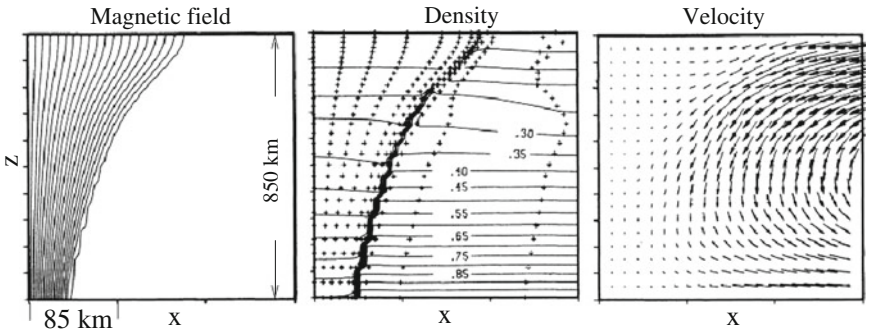

Fig. 2.4 Results of the slab modeling. **a** Lines of constant density normalized to $\rho_0 = 1.610^{-6}\,\mathrm{g\,cm^{-3}}$; the *crosses* indicate the location of the node points, concentrated at the edge of the slab where the steepest gradients appear. **b** Magnetic field lines. **c** Velocity field; maximum velocity is $\sim 200\,\mathrm{m\ s^{-1}}$. The horizontal scale is stretched by a factor 10/3 in order to show more details of the structure. Credit: Deinzer et al. (1984a, b), reproduced with permission ESO

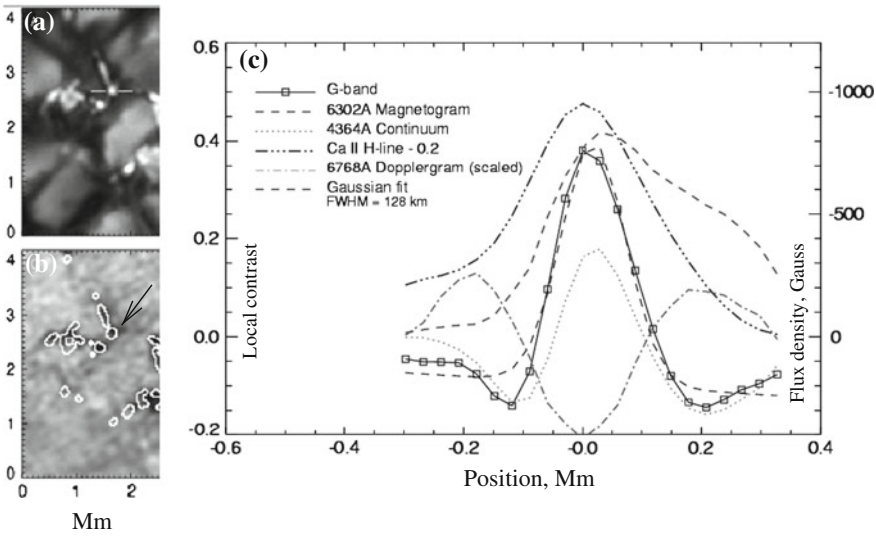

Fig. 2.5 Region containing a closely packed system of small scale magnetic element. *Top left* is G-band 4,305 Å filtergram and *bottom left* is magnetogram. The *white lines* highlight a *bright point* across which a relative intensity profiles are shown in *right panel*. Credit: Berger et al. (2004), reproduced with permission ESO

Figures 2.5 and 2.6 show results of the observations made with the Swedish 1-m Solar Telescope (SST) on La Palma (Scharmer et al. 2003), which may resolve the magnetic structures in the G-band 4,305 Å bandpass with 70 km resolution. Using the SST data, Berger et al. (2004) studied magnetic elements in a plage region near disk center. The SST data were complimented by a co-temporal Ca II H image, showing

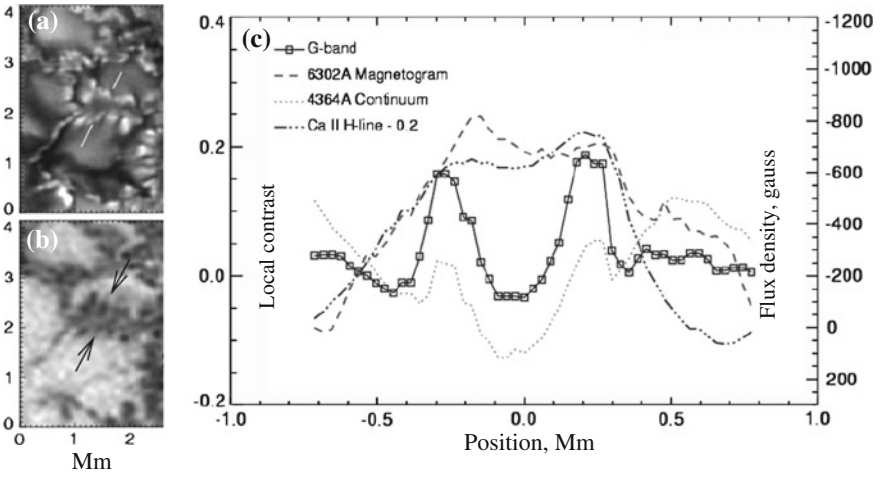

Fig. 2.6 The same as in Fig. 2.5 but for a region containing very small isolated bright point and elongated dark features. Credit: Berger et al. (2004), reproduced with permission ESO

the network elements in low chromosphere, and high-resolution magnetogram that resolves structures as small as 120 km with a flux sensitivity of $\simeq$130 Mx cm^{-2}. Figure 2.5 shows a 2.5 $\times$ 4 Mm sample region containing small scale magnetic elements which, at any moment of time fill intergranular lanes. Their lifetime is usually on the order of granular time scales ($\sim$8–10 min) or less. The top left panel shows G-band 4,305 Å filtergram and bottom left is magnetogram of the region. The white lines highlight a bright point across which intensities of several parameters were measured. These are shown in the right panel.

The solid curve with squares is the G-band intensity, duplicated by the Gaussian fit (dark dashed curve). The FWHM is 128 km. Also shown are plots of co-temporal and aligned data in the chromospheric Ca II H-line and 4,364 Å continuum with the corresponding magnetogram and Dopplergram signals. The peak absolute magnetic flux density is 836 Mx cm^{-2}. The peak downflow velocity measured in the Dopplergram slice is 543 m s^{-1}, displaced from the G-band peak emission by approximately 200 km on either side of the cut. This displacement of downflow velocity relative to the magnetic and bright point agrees well with the numerical models mentioned above (Deinzer et al. 1984a, b). This has been confirmed in later numerical simulations as well (e.g. Steiner et al. (1998)).

Figure 2.6 is another example of the same procedure as above but for the diverging ribbon-like structure which is not resolved into individual flux tubes. The measured magnetic flux density in the ribbon structures ranges from 300 to 1,500 Mx cm^{-2}.

As in the previous case, the chromospheric emission closely follows the G-band pattern and the magnetogram signal exhibits more discrete structures. The right panel shows a distinct double-peak shape in all of the emission lines indicating higher intensities and magnetic flux density at the edges of the ribbon structure. The maximum

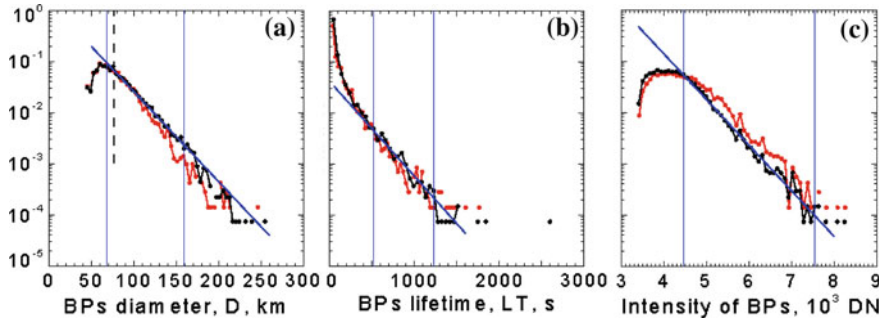

Fig. 2.7 Probability distribution functions of small scale magnetic features: **a** diameters, **b** lifetimes and **c** intensities. The data represent two sets of runs corresponding to lowest (*black*) and highest (*red*) threshold of intensity masks. *Straight blue lines* show the exponential fit showing a log-normal distribution of all the parameters. Courtesy of Abramenko, see also Abramenko et al. (2010)

absolute-value flux density in the bright point region is 1,341 Mx cm^{-2}. The magnetic flux density in the central region is also quite large, ~ -700 Mx cm^{-2}, indicating that this is a complex but rather symmetric magnetic body with a darkened interior and bright walls.

This kind of structures appeared in various numerical simulations studying formation of photospheric flux tubes, pores and light bridges (see e.g. Steiner (2007), Jafarzadeh et al. (2013) and literature therein). These studies are well facilitated by increasing possibilities of observations which include not only studies of individual flux tubes but their statistical properties as well.

Figure 2.7 shows an example of statistical studies performed with New Solar Telescope (NST) of Big Bear Solar Observatory. Observations were done with adaptive optics correction using TiO 7057 Å line with 10 s time cadence (Abramenko et al. 2010). Figure 2.7 shows the probability distribution functions (PDFs) for the diameter, D, lifetime, LT, and maximum intensity, $I_{\max}$, of bright points tracked during about 2 h period.

It was found that 98.6 % of bright points live less than 120 s. The lifetime distribution function follows a log-normal approximation for all features with lifetime exceeding 100 s. The longest registered life time was 44 min. The size and maximum intensity of BPs were found to be proportional to their lifetimes. A majority of bright points were found to be transient events reflecting the strong dynamics of the quiet sun populated by small scale magnetic flux tubes. The distribution function of their sizes extends to the diffraction limit of instrument, 77 km. The authors conclude that the *real minimum size of magnetic flux tubes has not yet been detected* in observations with modern high resolution telescopes.

As a building block of the solar magnetic fields, flux tubes play a major role in all physical processes in the sun from the energy production, its transfer and release to overall global behavior of the sun. Study of these processes and the flux tubes involvement in them is the subject of this book.

2.4 Filamentary Structures in Laboratory and Universe

The universe consisting of ever moving elementary particles and ionized gases is pierced by inborn magnetic fields. Highly advanced observations show their ubiquitous filamentary structure. But long before this fact became evident, in studies of laboratory plasma the *concept* of magnetic flux tubes became a necessity.

Invention of tokamak, and a possibility that magnetic field of the appropriate configuration could provide plasma confinement brought up the problems of plasma equilibrium and stability. This, in turn, lead to the concept of *magnetic flux tubes* (Rosenbluth and Longmire 1957; Spitzer 1958; Kadomtsev 1959). It has been realized that among the properties of the magnetic field that are needed for stable confinement of plasma, the essential role may be played by their filamentary structure (Leontovich 1965; Morozov and Solov'ev 1966; Leontovich 1966). Examples illustrating a possible configuration of flux tubes is shown in Fig. 2.8.

The concept of magnetic flux tube requires that on the surface on the tube $(\mathbf{n} \cdot \mathbf{B}) = 0$, where $\mathbf{n}$ is the normal to tube surface. Given that $\mathrm{div}\mathbf{B} = 0$, inside flux tube magnetic flux must be conserved, $\mathrm{d}\Phi = \mathbf{B}\mathrm{d}\mathbf{S}$; cf. (2.8) and (2.9).

Although magnetic field is divergence free, it was understood, that a flux tube can branch into two or more tubes. If line of force does not branch, then it cannot have a beginning or an end. Hence, it was postulated that there are three classes of nonbranching lines of force:

(1) those that start at infinity and end at infinity;
(2) those that remain in a bounded volume (closed or nonclosed) and
(3) field lines that originate at infinity but are trapped within a finite volume. These early studies of various magnetic field configurations and their properties form the basis for the studies of magnetic field structures and their effects on various plasmas. Since then, these studies went far beyond the tokamak devices, and, along the mainstream of creating energy producing devices, brought together laboratory and astrophysical plasmas.

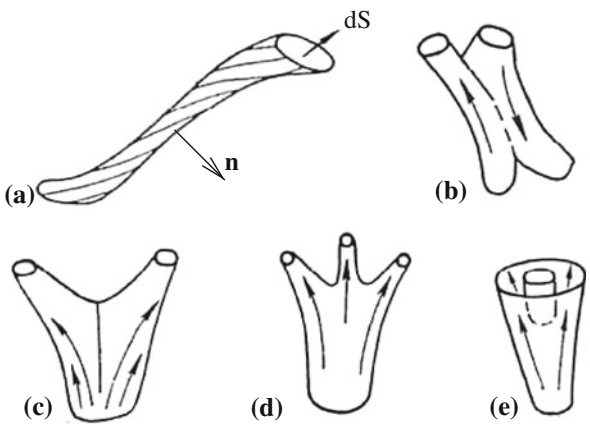

Fig. 2.8 The concept of magnetic flux tube. **a** The tube of a cross section d*S* and the normal to tube surface, **n**; **b**–**e** Several possibilities of branching of tube which occurs at singular points having different characters (after Morozov and Solov'ev (1966))

The laboratory experiment allows one to change characteristic parameters of the object and follow a time history of the event during desired time interval. It is remarkable that the laboratory experiments that deal with targets of a spatial scale from several μm to several cm and timescales of nanoseconds and seconds can reproduce phenomena occurring in stellar coronae, galactic jets, fine structures in supernovae remnants and solar atmosphere. Existence of a broad magnetohydrodynamic similarity (Ryutov et al. 2001; Ryutov and Remington 2007; Drake 2009) allows a direct scaling of laboratory results to astrophysical phenomena.

For the time being, a rich bank of encouraging results from laboratory experiments aimed to study the astrophysical plasma have been accumulated (Romero-Talamas et al. 2006; Lapenta et al. 2006; Bellan 2008; Perrone et al. 2013; Brown et al. 2014). As an example, in Fig. 2.9 we show the spheromak formation and evolution (Romero-Talamas et al. 2006), captured by a high-speed imaging system in the sustained spheromak physics experiment (SSPX) (Hooper et al. 1999; McLean et al. 2001). Spheromak is one of the topologically simplest "long-lived" configuration in the form of a compact toroid. Of many applications, spheromaks can be used, for

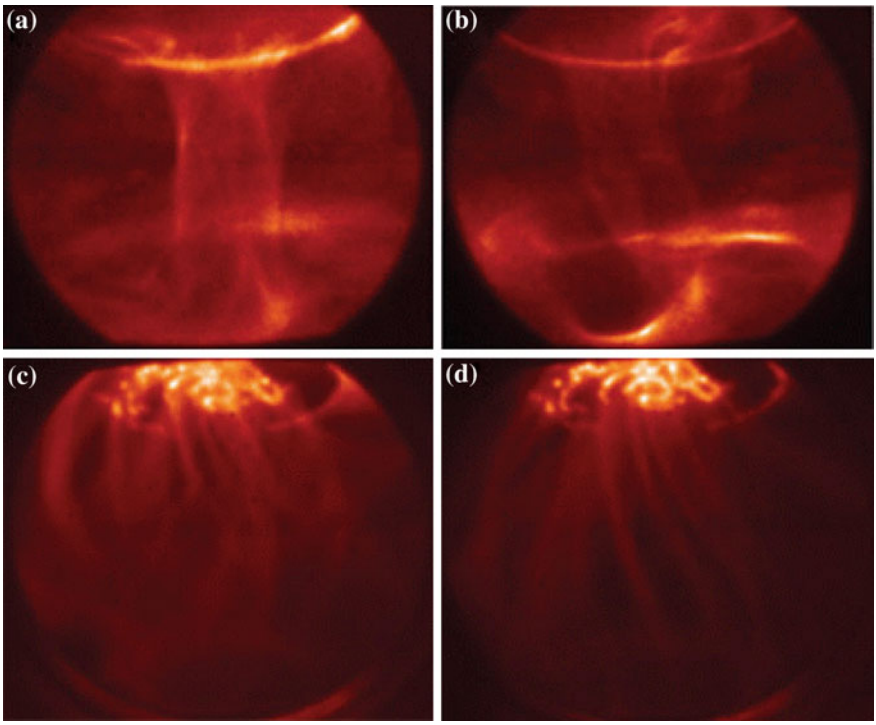

Fig. 2.9 Formation and evolution of a plasma column inside the spheromak: **a** Regime of a column formation (about 50 μs after the plasma injection). **b** At 80 μs the column acquires a *kinked shape*. **c** Regime of filamentation: central column becomes a messy collection of filaments. **d** Possible regimes of selforganization of filamentary structure (Courtesy of Harry McLean, LLNL, see also Romero-Talamas et al. (2006))

example, to study how electric currents in the plasma produce the spheromak, how it evolves and whether it is capable containing hot plasmas. In course of these studies it became clear that the observed regularities are often similar to phenomena observed in astrophysical plasmas, and in particular in the solar corona. Figure 2.9 shows four stages of the spheromak evolution. The plasma enters the high-speed camera field of view a few tens of microseconds after injection, and begins to balloon out of the injector gun. In about 50 μs the plasma reaches the bottom of the flux conserver and a column forms. This moment is shown in Fig. 2.9a. At 80 μs the column acquires a kinked shape (Fig. 2.9b). Toward the end of the plasma's lifetime, its central column becomes a collection of thin filaments and then reorganizes itself into a more regular system of filaments.

The process of filamentation and accompanying phenomena have numerous analogies from chemistry and discharge tubes to neutron stars and supernovae. Examples of two extreme objects pierced by "thin" filaments are shown in Fig. 2.10. Top panel shows a pulsed corona discharge in atmospheric air generated between a planar high-voltage electrode and the water surface with an immersed stainless steel plate electrode. During each pulse thin glow-like filaments were formed which then propagate along the gas–liquid interface (Lukes et al. 2011). Bottom panel shows a well-defined hairy structure of # 49 supernova remnant, typical to all the supernovae and their remnants.

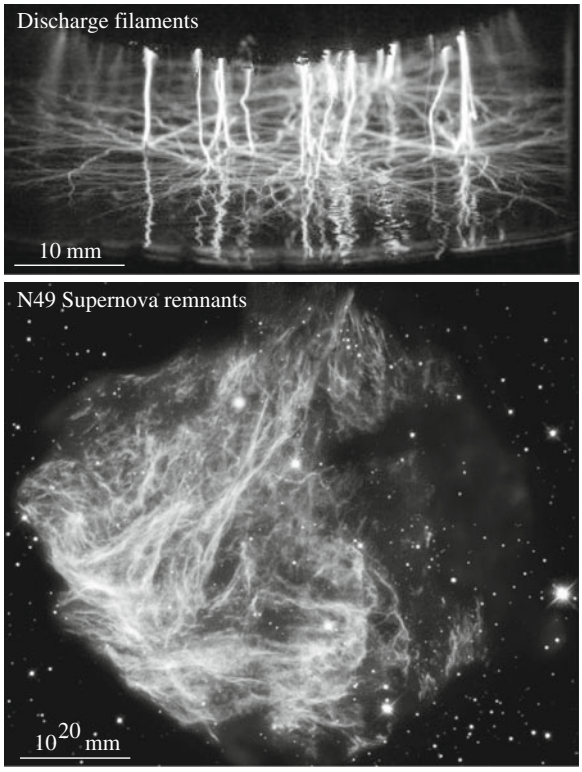

Fig. 2.10 Two extreme scales of filamentary structures. *Top* The gas discharge filaments generated along the water surface (courtesy of Petr Lukes); *Bottom* N49 supernova remnant located in the Large Magellanic Cloud taken by NASA's Chandra X-ray observatory (courtesy of NASA)

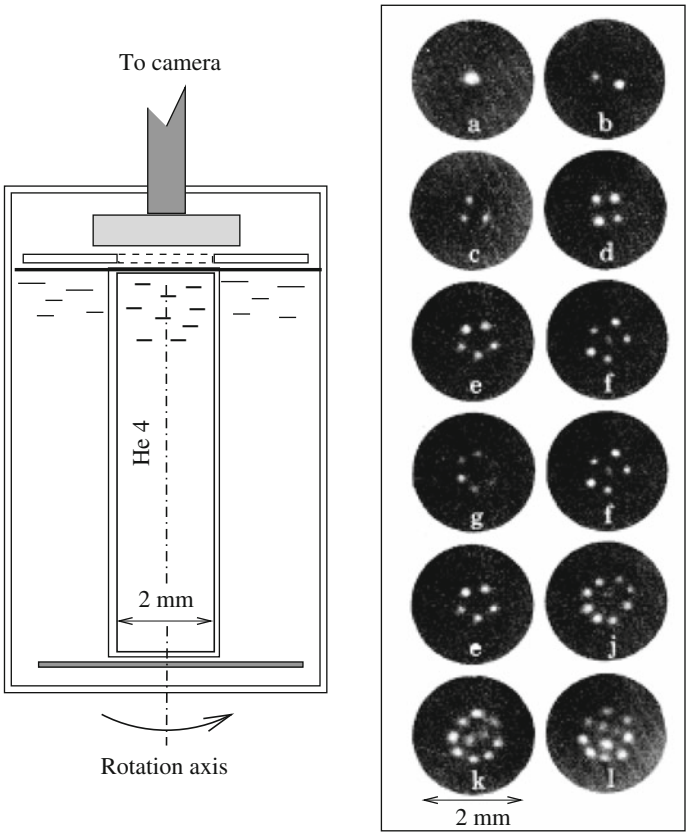

Fig. 2.11 Photographs of stable vortex arrays. *Left* Schematic of the experiment. *Right* Appearence of quantum vortices at different angular velocities of bucket. The diameter of the *dark circles* corresponds to the 2 mm bucket diameter. The angular velocities range from (*a*) $0.30\,\mathrm{s}^{-1}$ to (*l*) $0.59\,\mathrm{s}^{-1}$ with somewhat uneven intervals. Reprinted with permission from Yarmchuk et al. (1979). Copyright APS

We conclude this chapter by a fascinating and known for a long time examples of filamentary structures that were predicted and discovered as macroscopic quantum phenomena.

Long before the concept of magnetic flux tubes has been introduced in a tokamak plasma, in low temperature physics filamentation of substance became a starting point in studies of amazing phenomena in superfluidity and superconductivity (Landau 1941; Onsager 1949; Feynman 1955; Abrikosov 1957). A He 4 isotope below the 2.17 K (dabbed Helium II) becomes superfluid, but in various situations, such as under action of a heat or placed in a capillary tube, behaves as a mixture of a superfluid and normal components. A dual nature of Helium II is especially prominent when placed in a rotating cylinder. At some critical angular velocity there appear vortices with circulation quantized in units of h/m (h being a Planck's constant and m is the mass of the Helium atom).

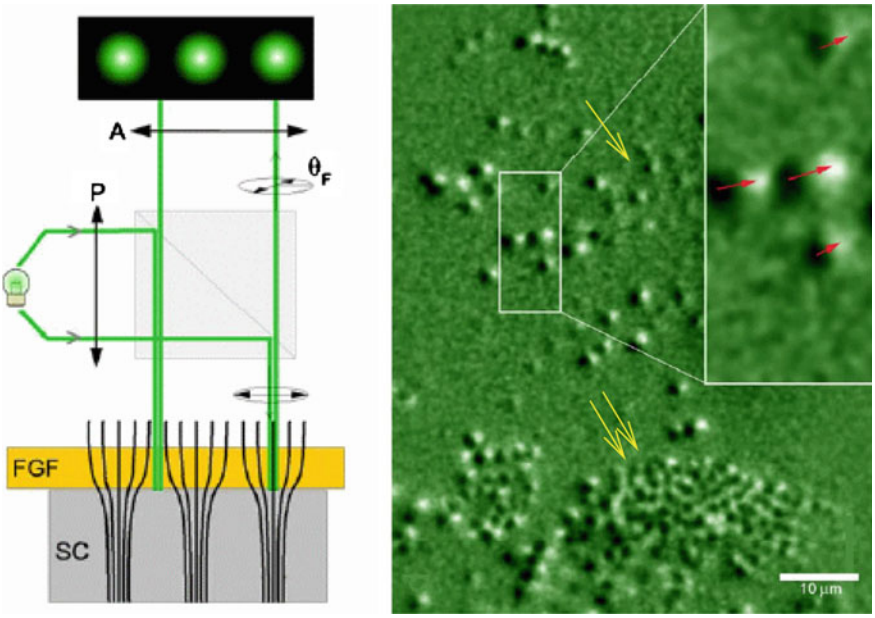

Fig. 2.12 Visualization of Abrikosov vortices and their dynamics in superconducting $NbSe_2$. *Left* Schematic of the experiment setting (see text for details). *Right* Magneto-optical images of vortices and their response to an increase of the applied magnetizing field by 4 mOe. The *dark* and *bright spots* represent initial and final vortex positions, respectively. The scale bar represents 10 μm. Reprinted from Goa et al. (2001) by permission from IOP Publishing

By the nature the vortices are the elements of a condensate: the vortex core consists of the *normal* component, and formation of vortices transforms the superfluid into the normal state. According to the theory, appearence of quantum vortices is energetically favorable. Moreover, in the established state the vortices have a minimal circulation (i.e., just h/m) and happen to form a regular lattice.

One of the first experiments demonstrating the formation of quantum vortices is shown in Fig. 2.11. One can see that with increasing the angular velocity of container there appear more and more vortices, just in agreement with theory predicting that in a container rotating at angular velocity ω, vortices should appear with a density $2\omega m/h$ (Feynman 1955). Tkachenko (1966) predicted that in equilibrium the vortices should form a triangular lattice. And they indeed do.

Filamentary processes occur as well in Bose-Einstein condensates (BEC, very cold atomic gases), He-3 isotope below 0.0025, and various types of superconductors.

Metals in superconducting phase having a zero resistivity are known to expel the magnetic field. The transition from superconducting to normal state usually has a discrete quantum nature. In Type-II superconductors, for example, such a transition occurs via formation of an Angstrom size threads that carry quantized magnetic flux, Abrikosov vortices (Abrikosov 1957).

With the improved experimental technique it became possible to observe individual vortices and their dynamics. Figure 2.12 shows a real-time imaging of Abrikosov vortices in superconducting $NbSe_2$ (Goa et al. 2001).

Left panel in Fig. 2.12 shows a principle of a high-sensitivity magneto-optical (MO) imaging. The maxima of the magnetic field from vortices in a superconducting sample (SC) give maxima in the Faraday rotation F of incoming plane polarized light, which shows up in a ferrite garnet layer (FGF) near the sample. Vortices appear as bright spots when imaged using a crossed polarizer, P, and analyzer, A. Right panel shows resulted vortex dynamics during flux penetration. The image shows the change in flux distribution over a 1 s time interval after a 4 mOe increase in the applied field. The dark and bright spots represent initial and final vortex positions, respectively. Medium brightness corresponds to an unchanged flux distribution, indicating stationary vortices. The insert shows a close-up view of four vortex jumps. The arrows indicate the direction of vortex motion. Note how close is a visual resemblence between the distribution of vortices and distribution of flux tubes over the solar surface: a "filling factor" of vortices changes from very small number where they form a rarefied ensembles (white arrow) to almost unity where vortices form a dense conglomerate (double white arrows).

Vortices in superfluid Helium and superconductors, magnetic flux tubes in solar atmosphere and space, filamentation process in biology and chemistry have probably a common ground, which is to be yet established. One conclusion can be made for sure: *formation of filamentary structures in nature is energetically favorable and fundamental process*.

References

V. Abramenko et al., Astrophys. J. **725**, L101 (2010)
A.A. Abrikosov, Sov. Phys. JETP **5**, 1174 (1957)
H.W. Babcock, H.D. Babcock, Astrophys. J. **121**, 349 (1955)
G. Batchelor, *An Introduction to Fluid Dynamics* (Cambridge University Press, Cambridge, 2000)
J.M. Beckers, E.H. Schröter, Sol. Phys. **4**, 142 (1968)
P.M. Bellan, *Fundamentals of Plasma Physics* (Cambridge University Press, Cambridge, 2008)
T.E. Berger, L.H.M. Rouppe van der Voort, M.G. Lfdahl et al., Astron. Astrophys. **428**, 613 (2004)
M.R. Brown et al., *Micro-physics of Cosmic Plasmas: Hierarchies of Plasma Instabilities from MHD to Kinetic* (Springer, Berlin, 2014)
L.E. Cram, P.R. Wilson, Sol. Phys. **41**, 313 (1975)
R.J. Defouw, Astrophys. J. **209**, 266 (1976)
W. Deinzer, G. Hensler, M. Schuessler, E. Weisshaar, Astron. Astrophys. **139**, 426 (1984a)
W. Deinzer, G. Hensler, M. Schuessler, E. Weisshaar, Astron. Astrophys. **139**, 435 (1984b)
R.P. Drake, Phys. Plasmas **16**, 5501 (2009)
R.P. Feynman, Progr. Low Temp. Phys. Chap. 2. **1** (1955)
E.N. Frazier, J. Stenflo, Sol. Phys. **27**, 330 (1972)
P.E. Goa et al., Supercond. Sci. Technol. **14**, 729 (2001)
R. Howard, Astrophys. J. **130**, 193 (1959)
R. Howard, J. Stenflo, Sol. Phys. **22**, 402 (1972)
E.B. Hooper, L.D. Pearlstein, R.H. Bulmer, Nucl. Fusion **39**, 863 (1999)
S. Jafarzadeh et al., Astron. Astrophys. **549**, 116 (2013)

B.B. Kadomtsev, *Plasma Physics and the Problem of Controlled Thermonuclear Reactions*, vol. IV (Pergamon Press, New York, 1959)
B.B. Kadomtsev, in *Reviews of Plasma Physics*, vol. 2, ed. by M.A. Leontovich (Consultants Bureau, New York, 1966), p. 153
M.D. Kruskal, R.M. Kulsrud, Phys. Fluids **1**, 265 (1958)
L.D. Landau, J. Phys. Mosc. **5**, 71 (1941)
G. Lapenta et al., JGR **111**, A12S06 (2006)
R.B. Leighton, Astrophys. J. **130**, 366 (1959)
M.A. Leontovich (ed.), *Reviews of Plasma Physics*, vol. 1 (Consultants Bureau, New York, 1965)
M.A. Leontovich (ed.), *Reviews of Plasma Physics*, vol. 2 (Consultants Bureau, New York, 1966)
W. Livingston, Nature **350**, 45 (1991)
P. Lukes, M. Clupek, V. Babicky, IEEE Trans. Plasma Sci. **39**, 2644 (2011)
H.S. McLean et al., Rev. Sci. Instrum. **72**, 556 (2001)
F. Meyer, H.U. Schmidt, N.O. Weiss, MNRAS **179**, 741 (1977)
A.I. Morozov, L.S. Solov'ev, in *Reviews of Plasma Physics*, vol. 2, ed. by M.A. Leontovich (Consultants Bureau, New York, 1966), p. 1
L. Onsager, Suppl. Nouvoo Cimento **6**, 249 (1949)
D. Papathanasoglou, Sol. Phys. **21**, 113 (1971)
E. Parker, Astrophys. J. **189**, 563 (1974a)
E. Parker, Astrophys. J. **190**, 429 (1974b)
E. Parker, in *Basic Mechanisms of Solar Activity, IAU*, ed. by V. Bumba, J. Kleczek (1976), p. 406
E. Parker, *Cosmical Magnetic Fields* (Oxford University Press, Oxford, 1979)
J.H. Piddington, Astrophys. Space Sci. **34**, 347 (1975)
J.H. Piddington, Astrophys. Space Sci. **55**, 401 (1978)
S.B. Pikel'ner, Sov. Astron. **6**, 757 (1963)
D. Perrone et al., SSRv. **178**, 233 (2013)
B. Roberts, A.R. Webb, Sol. Phys. **56**, 5 (1978)
C.A. Romero-Talamas et al., Phys. Plasmas **13**, 2502 (2006)
M.N. Rosenbluth, C. Longmire, Ann. Phys. **1**, 120 (1957)
B. Ruiz Cobo, K.G. Puschmann, Astrophys. J. **745**, 141 (2012)
D.D. Ryutov, M.P. Ryutova, Sov. Phys. - JETP **43**, 491 (1976)
D.D. Ryutov, B.A. Remington, H.F. Robey, R.P. Drake, Phys. Plasmas **8**, 1804 (2001)
D.D. Ryutov, B.A. Remington, Astrophys. Space Sci. **307**, 291 (2007)
M.P. Ryutova, in *Proceedings of the XIII-th International Conference on Phenomena in Ionized Gases*, p. 859 (1977)
M. Ryutova, T. Berger, A. Title, Astrophys. J. **676**, 1356 (2008)
V.D. Shafranov, At. Energy **30**, 38 (1956)
G. Scharmer, K. Bjelksjo, T. Korhonen, B. Lindberg, B. Petterson, in *Proceedings of SPIE in Innovative Telescopes and Instrumentation for Solar Astrophysics*, vol. 4853 ed. by S.L. Keil, S.V. Avakyan, p. 341 (2003)
A.B. Severny, Soviet Astronomy **3**, 214 (1959)
N.R. Sheeley Jr, Astrophys. J. **144**, 723 (1966)
N.R. Sheeley Jr, Sol. Phys. **1**, 171 (1967)
L. Spitzer in *Proceedings of 2-nd International Conference Atoms for Peace*. (Geneva 1958), p. 40
H.C. Spruit, Astron. Astrophys. **98**, 155 (1981)
O. Steiner, U. Grossmann-Doerth, M. Knoelker, M. Schuessler, Astrophys. J. **495**, 468 (1998)
O. Steiner, AIP Conf. Proc. **919**, 74 (2007)
J. Stenflo, Astron. Astrophys. Rev. **21**, 66 (2013)
N.V. Steshenko, Publ. Crime. Astrophys. Obs. **37**, 21 (1967)
J.T. Su et al., Astrophys. J. **710**, 170 (2010)
V.K. Tkachenko, Sov. Phys. JETP **23**, 1049 (1966)
E.J. Yarmchuk, M.J.V.R. Gordon, R.E. Packard, Phys. Rev. Lett. **43**, 214 (1979)

http://www.springer.com/978-3-662-45242-4

Physics of Magnetic Flux Tubes

Ryutova, M.

2015, XXII, 559 p. 231 illus., 60 illus. in color., Hardcover
ISBN: 978-3-662-45242-4